Green Chemistry

Accepted Manuscript

This article can be cited before page numbers have been issued, to do this please use: C. Huang, C. Yang, P. Gao, N. Wang, C. Chen and J. Chang, *Green Chem.*, 2015, DOI: 10.1039/C5GC00188A.

ROYAL SOCIETY OF CHEMISTRY

www.rsc.org/greenchem

View Article Online
DOI: 10.1039/C5GC00188A

Characterization of Alkaline Earth Metal-doped Solid Superacid and Activity for the Esterification of Oleic Acid with Methanol

Chien-Chang Huang*[a], Chieh-Ju Yang[a], Pei-Jyuan Gao[a], Nai-Ci Wang[a], Ching-Lung Chen[b] and Jo-Shu Chang[b]

Abstract

The leaching of grafted sulfate groups is one of the major issues for the solid acid catalysts with sulfate modification. A detailed study of sulfated alkaline earth metal-ferric composite oxides is investigated to suppress the leaching of sulfate groups as well as maintain high reactivity during the esterification of oleic acid. The acid properties and quantities of the active sites present on the catalysts were studied with pyridine-adsorption FT-IR, TGA, and titration methods. The following order of acidic strength was observed: SO_4^{2-}/Sr-Fe oxide > SO_4^{2-}/Ca-Fe oxide > SO_4^{2-}/Mg-Fe oxide. After sulfate modification, sulfate ions are linked to the composite oxides in a bridged bidentate form. SO_4^{2-}/Sr-Fe oxide exhibits superacidic nature due to the high induction effect of the sulfated ion grafted on Sr cation. TGA and FT-IR spectroscopic analyses provide new insights into the function of the iron cations implanted on the catalyst surface for enhancing the turnover frequency (TOF) of the active sites on SO_4^{2-}/Sr-Fe oxide in the esterification. It was verified that the active energy of SO_4^{2-}/Sr-Fe oxide for the esterification of oleic acid with methanol was as low as 28.53±0.72 kJmol^{-1}. In the reusability study, SO_4^{2-}/Sr-Fe oxide exhibited high reusability in the esterification, due to the high stability of the sulfate ion grafted on SO_4^{2-}/Sr-Fe oxide.

Keywords: Biodiesel, Alkaline earth metal ion, Oleic acid esterification, Sulfated composite oxide.

1. Introduction

Esterification is an important reaction for the preparation of flavor chemicals, drugs, perfumes, cosmetic ingredients, solvents and biofuels. For biodiesel production

[a] *Department of Cosmetic Science, Providence University, 200 Sec. 7, Taiwan Boulevard, Shalu Dist., Taichung 433, Taiwan. Fax: +886 42631 1167; Tel:+886 42632 8001 ext. 15411; E-mail: cchuang9@pu.edu.tw*

[b] *Department of Chemical Engineering, National Cheng Kung University, 1 University Road, Tainan 701, Taiwan. Tex: +886 6894 4496; Tel: +886 6275 7575; E-mail: changjs@mail.ncku.edu.tw*

View Article Online
DOI: 10.1039/C5GC00188A

in particular, the acid-catalyzed pre-esterification of the free fatty acids (FFA) present in low cost plant oils or waste cooking oils is a key step to decrease the level of FFA and prevent the saponification of the free fatty acids before the oil can be used in the base-catalyzed transesterification as a feedstock[1,2,3,4,5]. At the industrial level, the esterification reactions of fatty acids are performed in a homogeneously catalyzed reaction. Mineral acids, such as H_2SO_4 and H_3PO_4, are the conventional homogeneous catalysts, due to their high reactivity and low prices. However, their usage is limited because mineral acids accelerate the corrosion of the production equipments, and the residual catalysts are difficult to remove from the product stream. An extra purification step is thus required to remove the remaining strong acid in the products derived from homogeneously acid-catalyzed reactions.

Solid acid catalysts are environmentally benign substitutes for mineral acids to meet the needs of green chemistry technologies. Since the reaction is catalyzed on a solid-liquid interface, the used solid catalyst can be easily extracted from the reaction medium. The used catalysts can then be recovered by washing with solvents or calcining at an appropriate temperature. In these respects, ion-exchange resins[6,7], zeolites, as well as sulfated metal oxides[8,9,10,11,12,13] are the promising alternatives for mineral acids. Among the several solid acid catalysts that have been reported to date, sulfated metallic oxides are examples of highly acidic catalysts, and some of these were classified as superacids.

In recent years, much attention has been paid to sulfated metal oxides. Zirconia[8,9], titanium[10,11], tin oxide[12,13] and related oxides modified by sulfate groups are the most commonly examined solid acid catalysts in previous studies. It has been reported that these catalysts provide significant catalytic reactivity in the esterification of carboxylic acid with alcohols[14], transesterification of triglycerides with alcohols[15], Friedel-Crafts alkylation and acylation[13], oxidation of alkenes with hydrogen peroxide[16,17] and the skeletal isomerization of alkanes[18]. Sulfated zirconia is known as one of the strongest solid acid catalysts, and has been well studied due to its superacidic nature and consequent potential as a solid acid catalyst for numerous acid-catalyzing reactions[8,9,19,20]. In particular, sulfated zirconia shows superior reactivity for the esterification of fatty acids, and its reactivity is much higher than that of conventional mineral acids[21]. Sulfated zirconia consequently seems to be a good replacement for the mineral acids to carry out the esterification of FFA existing in low cost plant oils.

Although much effort has been devoted to investigating the catalytic properties of sulfated zirconia in the esterification of fatty acids with alcohols, sulfated zirconia has several drawbacks that make its utilization in biodiesel production difficult at the industrial scale. The major drawback is its short life time and easy deactivation.

View Article Online
DOI: 10.1039/C5GC00188A

Ardizzone *et al.* noted that the sulfate groups on zirconia are thermally and chemically unstable.[22] They stated that sulfated zirconia has poor resistance to hydrolysis and alcoholysis of the sulfate groups grafted on the zirconia surface. If the reaction medium contains a polar substance or water, then the sulfate groups quickly leach out as H_2SO_4 and HSO_4^- [2,23]. The deactivation of sulfated zirconia in the esterification of fatty acid is thus irreversible, and the leached sulfate groups also contaminated the product stream of esterification in the biodiesel production process[24].

Several developments are thus needed to aid the commercial introduction of sulfated metal oxide to the biodiesel production process. These improvements include aspects such as: enhancing the stability of the grafted sulfate groups to avoid their leaching in the reaction medium and in the recovery process; simplifying the separation of used solid acid catalyst from the production stream to reduce operational cost; lowering operation temperature by means of improving the reactivity; as well as extending the lifetime to meet the demand of green technologies, in order to maintain the reactivity during catalytic reaction. Therefore, an appropriate support for the sulfate group is thus needed in order to meet the demands for an ideal solid acid catalyst. Alkaline earth metal oxides have been reported as a base catalyst in the literatures. The strong basic character of strontium oxide is one of its best-known chemical properties. In our previous study, it was found that the composite oxide prepared by incorporating strontium in ferric oxide matrix (Sr-Fe oxide) exhibited high base-catalytic reactivity for the transesterification of plant oil with methanol[25]. However, Sr-Fe oxide is quickly poisoned by the free fatty acid usually present in waste cooking oil, because saponification takes place on the catalyst's surface. To the best of our knowledge, sulfated alkaline earth metal-ferric oxides have not yet been explored as an acid catalyst for use in esterification reactions. Three magnetic alkaline earth metal-ferric oxides were thus adopted in this work for the grafting of sulfate groups to study the resulting improvements in catalytic properties, and to simplify the separation procedure of the used catalyst from the reaction medium. The catalytic properties of sulfated composite oxides were examined in the esterification of oleic acid with methanol, and their acid properties were well characterized. Of particular interest is that sulfated strontium-ferric oxide is a superacid, and shows high reactivity and stability in the esterification process.

2. Experimental

2.1. Catalyst preparation

Three alkaline earth metal-ferric composite oxides (denoted as composite oxides), including strontium-ferric oxide (Sr-Fe oxide), calcium-ferric oxide (Ca-Fe oxide) and

View Article Online
DOI: 10.1039/C5GC00188A

magnesium-ferric oxide (Mg-Fe oxide), were prepared by co-precipitation. Iron (III) nitrate nonanhydrate (purity 99%), strontium nitrate (purity 98%), calcium (II) nitrate tetrahydrate (purity 98%), tetraethyl silicate (purity 99.96%) were purchased from Showa, Inc, while magnesium nitrate hexahydrate (purity 98%) was obtained from Alfa-Aesar. All the reagents were commercial available and used as received. In a typical preparation, alkaline earth metal nitrate and iron (III) nitrate nonanhydrate in the desired molar ratio were pre-mixed in 80 ml of deionized water. 100 ml of 15 wt% ammonia hydroxide (from Fisher Science Inc.) was subsequently added into the solution drop by drop under vigorous stirring, and then aged at room temperature for 12 hours. The solid products which were obtained from the solutions by completely evaporating the liquid phases of the reactions at 85^{o}C were then calcined at 1100^{o}C for 10 hours. Sulfated strontium-ferric oxide (SO_4^{2-}/Sr-Fe oxide), sulfated calcium-ferric oxide (SO_4^{2-}/Ca-Fe oxide) and sulfated magnesium-ferric oxide (SO_4^{2-}/Mg-Fe oxide) were prepared by mixing 5g composite oxide with 100ml of 2M H_2SO_4 aqueous solution at room temperature for 2 hours, and then the sulfated solids were heat-treated at 400^{o}C for 2 hours to remove weakly bonded sulfate groups or unbonded sulfuric acid.

Three reference samples, SO_4^{2-}/Fe_2O_3, SO_4^{2-}/ZrO_2 and SO_4^{2-}/SrO, were also employed for the present experiments. Fe_2O_3 was prepared by precipitation of ferric hydroxide in a solution consisting of 38.17g iron (III) nitrate and 100 ml water by adding 100 ml 15% ammonium hydroxide into the solution drop by drop, and then calcined at 1100^{o}C for 10 hours. Subsequently, 1 g of the Fe_2O_3 was dispersed in 20 ml 2M H_2SO_4 aqueous solution under stirring for 2 hours. ZrO_2 particles were obtained following the method published by Fu *et al.*[15]. ZrO_2 was prepared by precipitation of zirconium hydroxide in the solution containing 10.31g zirconium (VI) oxychloride octahydrate ($ZrOCl_2 \cdot 8H_2O$) and 160ml H_2O by adding 30ml 30% ammonia hydroxide into the solution drop by drop, followed by calcinating at 600^{o}C for 8 hours. Sulfate groups were then grafted on the resulting ZrO_2 by immersing 1 g ZrO_2 in 20 ml 0.5M H_2SO_4 aqueous solution under stirring for 2 hours. The preparation method for obtaining SO_4^{2-}/SrO is similar to that of SO_4^{2-}/ZrO. 50 ml 30% ammonia hydroxide was added into the solution consist of 29.62 g strontium nitrate and 50 ml H_2O drop by drop. SrO was obtained by calcining the resulting particles obtained from the solution at 1100^{o}C for 10 hours. Sulfate groups were incorporated on SrO surface by mixing 1g SrO in 20ml 2M H_2SO_4 aqueous solution under stirring for 2 hours. The XRD pattern of SO_4^{2-}/SrO is shown in Figure S1. All sulfated reference samples were calcined at 400^{o}C for 2 hours prior to use.

SiO_2 powder for the Koros-Nowak test was synthesized using a modified Ströber process[26]. In general, 10 ml tetraethyl silicate (98% from Seedchem Co.) was added in

View Article Online
DOI: 10.1039/C5GC00188A

the mixture consisting of 66 ml iso-propanol (99% from Sigmaaldrich Co.), 4.1ml ammonium hydroxide (30% from Showa, Inc.) and 10ml de-ionized water under vigorous magnetic stirring. The reaction of which was allowed to proceed at room temperature (25^{o}C) for 10 hours. The resulting particles were separated from the reaction medium by vacuum filtration using filter paper and subsequently washed with de-ionized water twice, and were then dried at 110^{o}C in an oven for 12 hours.

2.2. Catalyst characterization

The specific surface areas of the sample catalysts were determined through the isothermal model of Brunauer-Emmett-Teller (BET) using a PMI Sorptometer CBET-201A. The XRD patterns were obtained by using a Rigaku Ultima IV X-ray diffractometer with Cu K_{α} radiation operated at 40 kV and 40 mA in the range of diffraction 2θ=10-90^{o} with a sweep rate of 1 degree/minute. The elemental composition and surface morphology of the catalyst samples were analyzed with a scanning electron microscope (SEM) equipped with an energy dispersive spectroscope (EDS) (JEOL Co. Ltd. JSM-7000F). A JASCO Asia Portal FT/IR-4100 spectrometer was utilized to obtain the FT-IR spectra of the samples by using the conventional KBr-pellet technique. Thermogravimetry analysis (TGA) was performed on a Perkin Elmer TGA7. About 5 mg of sample was heated at 10^{o}C/min from room temperature to desired temperature under a flowing stream of air while the associated weight loss was recorded.

2.3. Total acidity determination

The total acidity for all synthesized catalysts was determined by the n-butyl amine titration method[27]. In a typical procedure, 50 ml 0.025M solution of n-butyl amine (from Tedia) in toluene (from Echo) was pre-mixed with 0.5g of catalyst overnight at room temperature. The excess base was then back titrated by trichloroacetic acid (from Merck) using neutral red as an indicator. N-butyl amine is a strong base, and it was expected that n-butyl amine adsorbed on acid sites with various acid strengths. By back titrating the free n-butyl amine left in the solution after the acid sites saturated by n-butyl amine, the total number of acid sites present on the catalyst surface can be estimated.

2.4. Acid properties

The acidic properties of the sample catalysts were determined by the Hammett indicators and an infrared spectroscopic investigation of pyridine adsorbed on the samples. The indicators used in the present work were Dicinnamalacetone (pK_a=-3.0), anthraquinone (pK_a=-8.2), p-Nitrotoluene (pK_a=-11.35), p-Nitrochlorobenzene

View Article Online
DOI: 10.1039/C5GC00188A

(pK_a=-12.70) and 2,4-Dinitrotoluene (pK_a=-13.75). In the typical procedure for determining the acidic strength, 0.1g sample was pre-treated at 120^{o}C for 5 hours, and 0.1 wt% Hammett indicator diluted in toluene was then mixed with the sample in a sealed sample vial. The acidic strength of the sample was determined by the change in color of the indicators with different pK_a. The nature of acid sites (Brönsted or Lewis) was distinguished by infrared spectroscopic investigation of pyridine adsorbed on the sample. The sample in a U shape sample tube was pre-treated in N_2 stream at 400^{o}C for 2 hours, and then connected with the pyridine vapor. After this, the IR spectra of the pyridine vapor treated samples were recorded in a JASCO Asia Portal FT/IR-4100 spectrometer using KBr pellets.

2.5. Esterificaiton activity

The catalytic reactivity of the synthesized catalysts was evaluated in the esterification of oleic acid (from Aldrich) with methanol (from Echo) in a molar ratio of 1:4 at 100^{o}C. The test reaction was carried out in a sealed 100 ml batch reactor equipped with magnetic stirring. Oleic acid was pre-mixed with a weighted sample catalyst (10 wt% based on the weight of oleic oil), followed by methanol. The progress of the reaction was monitored by periodically withdrawing samples from the reaction mixture. The conversion of oleic acid was analyzed on a gas chromatograph (Shimadzu GC-2010) equipped with an Agilent^{TM} capillary column DB-5HT (15 m $\times$ 0.53 mm $\times$ 0.5 μm) and a flame ionization detector using N_2 as the carrier gas. The catalytic reactivity of the catalysts were evaluated by turnover frequency (TOF). TOF is defined as the turnover number (TON) per unit time, and TON is defined as mole of oleic acid converted in the reaction per mole of active site.

2.6. Recycling test

The reusability as well as the stability of the catalysts were tested by carrying out repeated cycles of the reaction at 100^{o}C for 2 hours. After performing the reaction over a catalyst, the catalyst was washed with hexane and subsequently calcined at 400^{o}C under air atmosphere. The recovered catalyst was then reloaded in the reactor with fresh reagents.

3. Results and Discussion

3.1 Characterization

3.1.1 XRD pattern

The crystalline phases of three sulfated composite oxide samples were carried

View Article Online
DOI: 10.1039/C5GC00188A

out by power X-ray diffraction (XRD), and their XRD patterns are shown in Figure 1. It reveals that these samples are crystalline materials, and no intense bands relating to the crystalline forms of the alkaline earth metal oxides are observed in the XRD patterns, indicating that the alkaline earth metal ions highly disperse in the catalysts. The obtained phases of SO_4^{2-}/Ca-Fe oxide and SO_4^{2-}/Mg-Fe oxide are indexed as spinel $CaFe_2O_4$ (JCPD No: 32-0168) and spinel $MgFe_2O_4$ (JCPD No: 17-0465), respectively, while the XRD pattern of SO_4^{2-}/Sr-Fe oxide is indexed as $Sr_7Fe_{10}O_{22}$ in the standard data (JCPD No: 26-0980). The atomic ratio of ferric ion to alkaline earth metal ion (Fe/M) determined by EDS for SO_4^{2-}/Sr-Fe oxide, SO_4^{2-}/Ca-Fe oxide and SO_4^{2-}/Mg-Fe oxide are 1.45, 2.45 and 3.35, respectively. Obviously, the Fe/M ratio determined by EDS are different from the stoichiometry of the phases detected by XRD for all sulfated composite oxides, implying the presence of another crystalline phase. Except for the crystalline phases of the composite oxides that were identified, another crystalline phase present in the XRD patterns of all sulfated composite oxide samples is indexed as Fe_2O_3 (JCPD No: 33-0664). The XRD traces for the SO_4^{2-}/Sr-Fe oxide samples with various Fe to Sr atomic ratios are shown in Figure 2. When the Fe/Sr ratio is in the range of 1.45 (SO_4^{2-}/Sr-Fe oxide-1) to 3.33 (SO_4^{2-}/Sr-Fe oxide-3), a fall in the Sr moiety does not lead to a change in the crystalline phase of SO_4^{2-}/Sr-Fe oxide. When Fe/Sr ratio is as high as 34.58 (SO_4^{2-}/Sr-Fe oxide-4), only the crystalline phase of Fe_2O_3 (JCPD No: 33-0664) is identified.

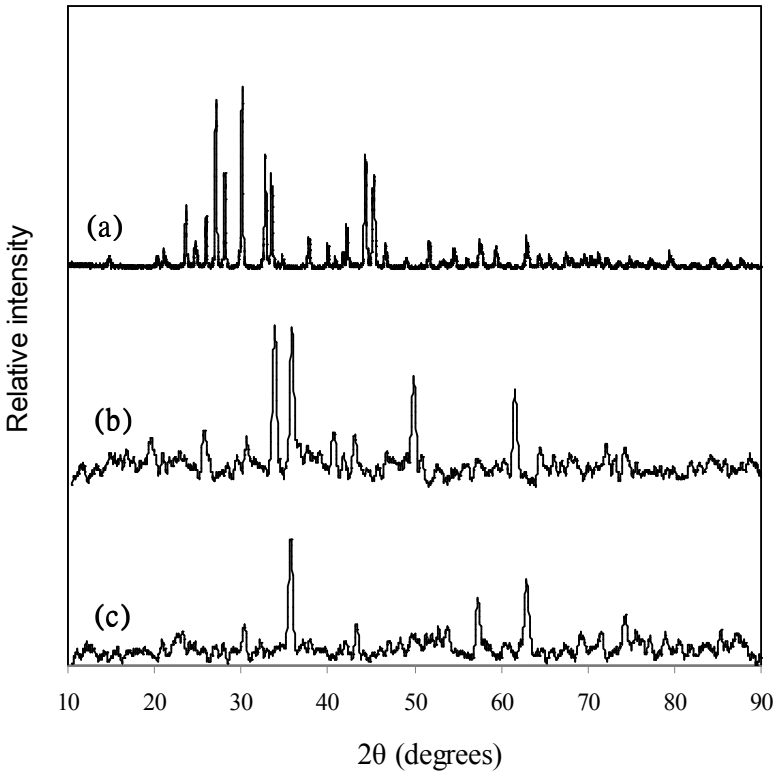

View Article Online
DOI: 10.1039/C5GC00188A

Figure 1. Powder X-ray patterns for (a) SO_4^{2-}/Sr-Fe oxide; (b) SO_4^{2-}/Ca-Fe oxide and (c) SO_4^{2-}/Mg-Fe oxide

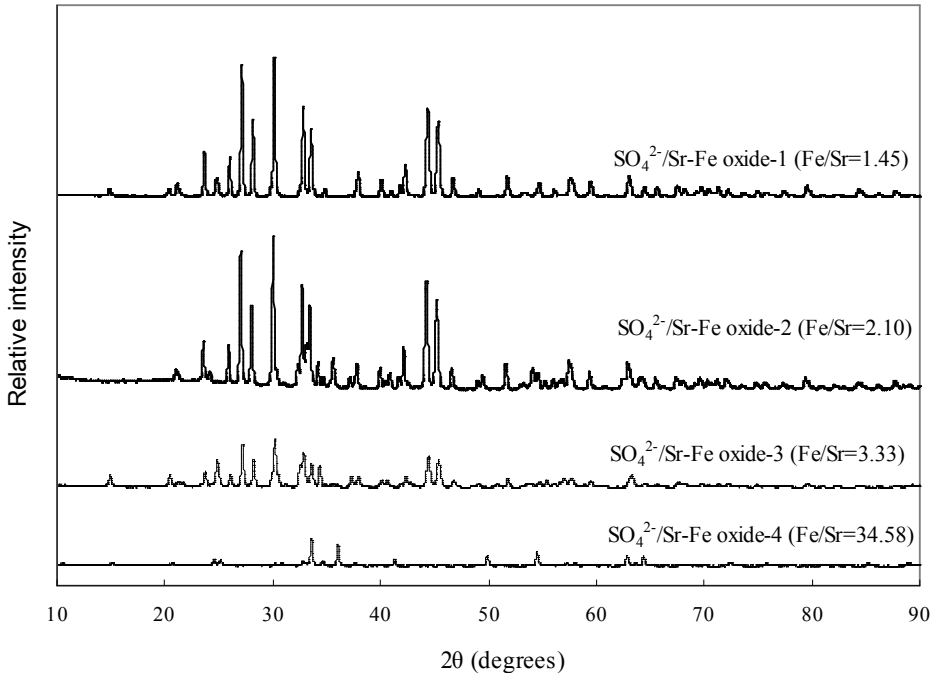

Figure 2. Powder X-ray patterns for SO_4^{2-}/Sr-Fe oxide samples with various Sr to Fe atomic ratio. The atomic ratio of Fe to Sr for all SO_4^{2-}/Sr-Fe oxide samples were determined by EDS analysis.

3.1.2 FT-IR spectra of sulfated composite oxides

The sulfate ions coordinated to the composite oxides were identified by FT-IR. The spectra are shown in Figure 3. With respect to the structure of sulfate ions, the sulfate ion in free form has T_d symmetry (Scheme 1(a)), with an intense IR band at around 1100 cm^{-1}. When a sulfate ion chemically bonds to the composite oxide's surface, the sulfate ion has C_{2v} symmetry (Scheme 1(b) and 1(c))[29]. As seen in Figure 3(a), the IR spectrum of SO_4^{2-}/Sr-Fe oxide shows four IR bands in the range of 1230 - 990 cm^{-1}. However, these IR bands were absent in the spectrum of the Sr-Fe composite oxide without sulfate modification, indicating that the IR bands in the range of 1230-990 cm^{-1} are associated with the covalently bonded sulfate ions, and the coordination of sulfate ions on the catalyst surface leads to a change in its configurations. The bands at 1225 cm^{-1} and 1130 cm^{-1} can be assigned to the asymmetric and symmetric stretching of the S=O bond, respectively. In addition, the bands at 1076 cm^{-1} and 995 cm^{-1} are attributed to the asymmetric and symmetric stretching of S-O bonds[11,28,29]. With regard to the structure of the adsorbed sulfate

View Article Online
DOI: 10.1039/C5GC00188A

group on metal oxides, there are two possible forms that have been reported in the literatures, bridged bidentate and chelating bidentate[30,31,32]. According to the IR bands of the sulfate ions on SO_4^{2-}/Sr-Fe oxide, it can be proposed that SO_4^{2-} groups covalently bonded to Sr-Fe oxide surfaces by the bridged bidentate form, in which sulfate group bridges across two metal ions[28] (Scheme 1(c)). The absence of the band around 1400 cm^{-1} reveals that a further reaction between adjacent sulfate groups, which would result in the formation of polynuclear sulfate $S_2O_7^{2-}$, did not take place[33]. An additional band at 1636 cm^{-1} corresponds to O-H bending of molecular water. The IR spectrum of SO_4^{2-}/Ca-Fe oxide and SO_4^{2-}/Mg-Fe oxide are also shown in Figure 3 (spectrum (b) and (c)). Their IR spectra show similar IR bands to the IR spectrum of SO_4^{2-}/Sr-Fe oxide in the range of 1230-900 cm^{-1}, indicating the presence of sulfate groups with the bridged bidentate structure on their surfaces.

The relative thermal stability of the coordinated sulfate ions on three sulfated composite oxides was also examined by FT-IR after pre-treating the samples at 700°C. The IR spectra are also shown in Figure 3 (from spectrum (a') to (c')). It is obvious that pre-treating the samples at 700°C leads to a change in their IR spectra, especially for SO_4^{2-}/Mg-Fe oxide. After pre-treating SO_4^{2-}/Mg-Fe oxide at 700°C for 2 hours, the IR spectrum of pre-treated SO_4^{2-}/Mg-Fe oxide does not show any IR bands related to sulfate ions, indicating a complete removal of the bonded sulfate groups (Figure 3 spectrum (c')). In contrast, pre-treating SO_4^{2-}/Sr-Fe oxide and SO_4^{2-}/Ca-Fe oxide at 700°C for 2 hours only diminishes the band intensities of sulfate ions (Figure 3 spectrum (a') and spectrum (b')). These results reveal that the residual sulfated ions on the SO_4^{2-}/Sr-Fe oxide and SO_4^{2-}/Ca-Fe oxide samples have high thermal stability, and the thermal stability of the adsorbed sulfate ions is associated with the alkaline earth metal ions implanted on the catalysts.

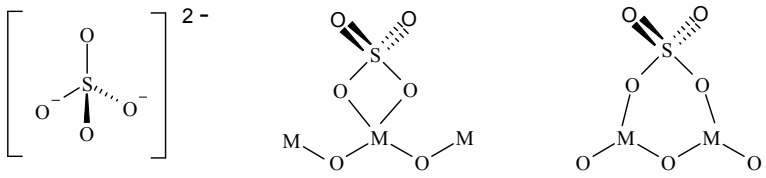

Scheme 1. The structure of (a) free sulfate ion with T_d symmetry, (b) bonded sulfate ion with chelate bidentate configuration, and (c) bonded sulfate ion with bridged bidentate configuration [29].

View Article Online
DOI: 10.1039/C5GC00188A

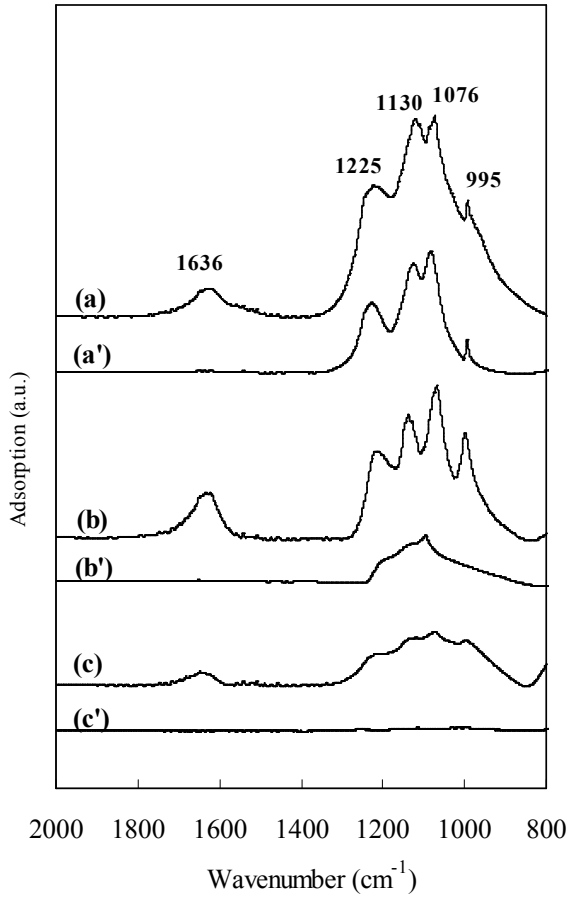

Figure 3. Infrared spectra of (a) SO_4^{2-}/Sr-Fe oxide; (b) SO_4^{2-}/Ca-Fe oxide and (c) SO_4^{2-}/Mg-Fe oxide, and the infrared spectra of heat-treated (a') SO_4^{2-}/Sr-Fe oxide, (b') SO_4^{2-}/Ca-Fe oxide and (c') SO_4^{2-}/Mg-Fe oxide at 700°C for 2 hours.

3.1.3 Textural properties of the coordinated sulfate ions on the catalysts

The TGA analyses of the sulfated composite oxides were carried out in air, and the profiles are shown in Figure 4. The initial weight loss on the TGA profiles is assigned to desorption of physically adsorbed water (100-200°C). Further, increasing the temperature from 250 °C to 600°C leads to gradual weight loss, associated with the removal of surface hydroxyl groups and carbonates, since most adsorbed hydroxyl groups and carbonates become thermally unstable before 600°C on metal oxides[28,34]. The significant weight loss that started at 600°C for all the catalyst samples is due to the decomposition of adsorbed sulfate ions (600-700°C). This is a typical feature for the TGA profiles of sulfated metal oxides[35]. Based on the TGA profiles, when the temperature increased from 600 to 700°C, the percentages of the weight of the sulfate ions eliminated from SO_4^{2-}/Sr-Fe oxide, SO_4^{2-}/Ca-Fe oxide and SO_4^{2-}/Mg-Fe oxide

View Article Online
DOI: 10.1039/C5GC00188A

are estimated to be 8.8% (w/w), 5.5% (w/w) and 2.5% (w/w), respectively.

Table 1 represents the acid site density estimated by TGA analysis (D_{TGA}) and by the n-butyl amine titration method (D_{BAT}). The IR spectrum of SO_4^{2-}/Mg-Fe oxide shown in Figure 3 indicates that heat-treating SO_4^{2-}/Mg-Fe oxide at 700°C leads to complete removal of adsorbed sulfate ions. According to the TGA profiles of SO_4^{2-}/Mg-Fe oxide (Figure 4), the density of the sulfate groups (S_{ion}) grafted on SO_4^{2-}/Mg-Fe oxide can thus be calculated. It is assumed previously that the sulfate group binds to Mg-Fe oxide in the bridged bidentate form, illustrating that the density of the acid sites is about two-fold the density of the bonded sulfate ions. Therefore, the acid site density can be estimated from S_{ion}. As seen in Table 1, the acid site density determined by TGA analysis (D_{TGA}) is close to that determined by the n-butyl amine titration method (D_{BAT}) for SO_4^{2-}/Mg-Fe oxide. This result is in agreement with the configuration of the adsorbed sulfate groups deduced from the IR bands shown in Figure 3, in which the sulfate group binds to the composite oxide by the bridged bidentate form.

The proposed configurations of the adsorbed sulfate groups on SO_4^{2-}/Sr-Fe oxide and SO_4^{2-}/Ca-Fe oxide are also deduced from the IR spectra shown in Figure 3 and the difference between S_{ion} and D_{BAT} shown in Table 1. As seen in Figure 3, the IR spectra show that a small fraction of sulfate ions remained on SO_4^{2-}/Sr-Fe oxide and SO_4^{2-}/Ca-Fe oxide after 700°C calcination. Figure 4 shows that no obvious weight loss was found on the TGA profiles of SO_4^{2-}/Sr-Fe oxide and SO_4^{2-}/Ca-Fe oxide when the temperature is over 700°C. The residual sulfate ions on the heat-treated catalysts can be classified as the sulfate groups with high thermal stability. D_{BAT} represents the density of the active sites actually present on catalyst surface. With respect to the configuration of the bonded sulfate ions on SO_4^{2-}/Sr-Fe oxide and SO_4^{2-}/Ca-Fe oxide, S_{ion} should be close to D_{BAT} if the sulfate groups bond to the catalyst surfaces by chelating bidentate form. However, the D_{BAT} of SO_4^{2-}/Sr-Fe oxide or SO_4^{2-}/Ca-Fe oxide is about 3 folds higher than the S_{ion}, suggesting that most sulfate ions bond to Sr-Fe oxide and Ca-Fe oxide by bridged bidentate form. According to the proposed configuration of bonded sulfate group, the density of the sulfate groups with high thermal stability can thus be calculated as 4.29×10^{-2} and 3.69×10^{-2} mmol/m^2 on SO_4^{2-}/Sr-Fe oxide and SO_4^{2-}/Ca-Fe oxide, respectively. The distribution of Lewis and Brönsted acid sites on the catalysts was investigated via pyridine FT-IR analysis (Figure S2). It was found that both Lewis and Brönsted acid site are present on SO_4^{2-}/Sr-Fe oxide and SO_4^{2-}/Ca-Fe oxide. Their configurations are proposed as indicated in Scheme 2(a). The ratio of the Brönsted acid sites to Lewis acid sites (N_B/N_L) estimated from the integral area under the specific bands shown in Figure S2 discloses that Brönsted acid sites dominate on SO_4^{2-}/Sr-Fe oxide and SO_4^{2-}/Ca-Fe

View Article Online
DOI: 10.1039/C5GC00188A

oxide. Therefore, the configuration of most active sites present on SO_4^{2-}/Sr-Fe oxide and SO_4^{2-}/Ca-Fe oxide can be proposed as the model shown in Scheme 2(b).

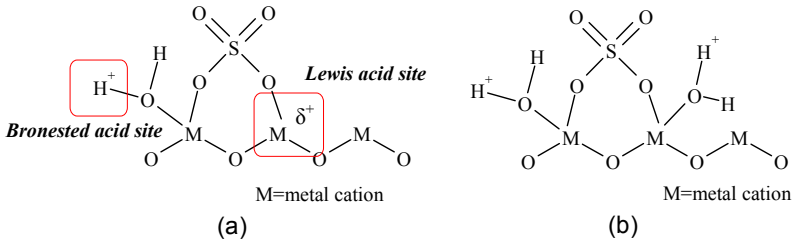

(a) (b)

Scheme 2. Schematic diagram of the sulfate group grafted on an alkaline earth metal-ferric oxide.

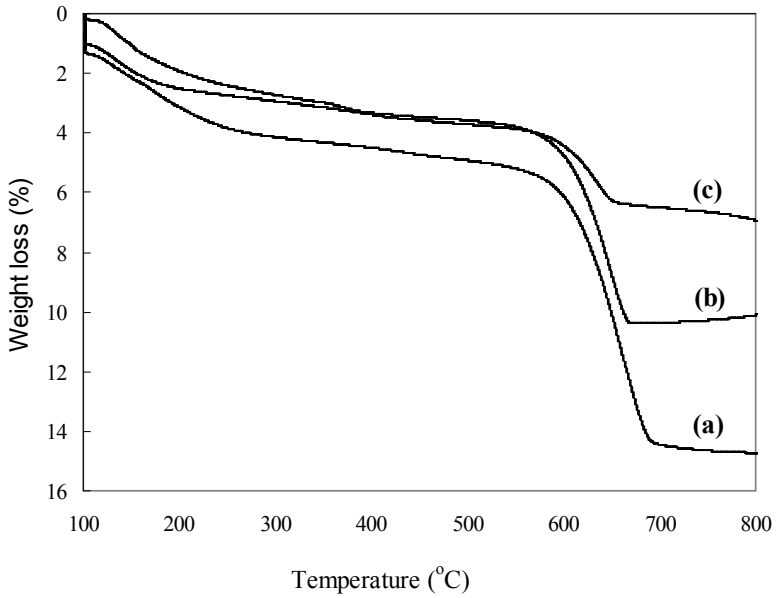

Figure 4. TGA profiles in air of (a) SO_4^{2-}/Sr-Fe oxide, (b) SO_4^{2-}/Ca-Fe oxide and (c) SO_4^{2-}/Mg-Fe oxide

Table 1. Acidic density of sulfated composite oxides determined by TGA (D_{TGA}) and by the n-butyl amine titration (D_{BAT})

catalyst	Area[a] (m^2/g)	TGA analysis			n-butyl amine titration	
		W_S content[b] ($\times10^{-2}$ g/g cat.)	S_{ion} density[c] ($\times10^{-2}$ mmol/m^2)	D_{TGA}[d] ($\times10^{-2}$ mmol/m^2)	Acidity (mmol/g)	D_{BAT}[e] ($\times10^{-2}$ mmol/m^2)
SO_4^{2-}/Sr-Fe oxide	9.47±0.21	9.00±0.28	9.90±0.09	19.80[f]	2.69±0.07	28.38±0.07
SO_4^{2-}/Ca-Fe oxide	10.7±0.54	5.35±0.21	5.21±0.06	10.42[f]	1.90±0.02	17.80±0.75
SO_4^{2-}/Mg-Fe oxide	4.87±1.04	2.85±0.50	6.13±0.25	12.26	0.60±0.11	12.43±0.46

[a] BET specific surface areas of sulfate modified catalysts

View Article Online
DOI: 10.1039/C5GC00188A

[b] sulfate ion weight per gram catalyst

[c] sulfate ion density on catalyst surface

[d] acid site density estimated via TGA analysis

[e] acid site density evaluated by using the n-butyl amine titration method

[ps.] the associated error and error bar in the tables and the figures were obtained by using the equation of Standard Deviation (SD)

$$SD = \sqrt{\frac{\sum (X - M)^2}{n - 1}}$$

Where X refers to the individual data, M is the mean of the data and n is number of data points.

3.1.4 Acid properties

The acidic strength is expressed by the Hammett acidity function, H_0. It was reported by Gillespie *et al.* that the acidic strength of 100% H_2SO_4 was H_0=-11.93[36]. When the H_0 of any solid acid is less than -11.93, the solid acid is known as a superacid. As the results show in Table 2, all the sulfated composite oxides exhibit remarkably high acidity, and particularly SO_4^{2-}/Sr-Fe oxide can be claimed to presence of superacid sites. The results of the Hammett indicator analysis demonstrate that there is a direct correlation between the acidic strength of the active sites and the alkaline earth metal ions incorporated to the catalysts. This observation is in agreement with the results of the pyridine FT-IR analysis, where SO_4^{2-}/Sr-Fe oxide shows higher binding ability for pyridine than the others. It seems that the acidic strength of the three sulfated composite oxides increases along with the difference in electronegativity between oxygen anions and the adjacent metal cations. The presence of superacid sites only on SO_4^{2-}/Sr-Fe oxide may be because the surface sulfate ions bound to the metal ions with a low electronegativity (Sr). The inductive effect of S=O of the sulfate ions makes the Lewis acid strength of Sr stronger, since it is easier for the bonded sulfate ion to pull covalent electrons away from the Sr ions. Once the Lewis site is converted to a Brönsted acid site via the covalent binding of water to the same Sr ion, the high acid strength character enables the Brönsted acid site to transfer a neutral Hammett base with a lower H_0 into its conjugate acid (BH^+).

To have a better understanding of the correlation between the incorporated alkaline earth metal cations and the acid site density, a series of strontium-ferric composite oxides with various Sr to Fe atomic ratios were prepared. The surface atomic ratios measured by EDS for each Sr-Fe composite oxide sample are shown in Table 3. In Table 3, the density of the acid sites is proportional to that of the Sr ions incorporated on catalyst surface, revealing that the surface Sr ions facilitate the binding of sulfated groups. Thus, when the catalyst surface is rich in Sr ions, more

View Article Online
DOI: 10.1039/C5GC00188A

acid sites are created after sulfate modification.

Table 2. Acidic strength of the sulfated composite oxides classified by the Hammett indicators

Catalyst	EN[a]	D_{EN}[b]	H_0[37]				
			-3.00	-8.20	-11.35	-12.70	-13.75
SO_4^{2-}/Sr-Fe oxide	0.963	2.647	+	+	+	+	-
SO_4^{2-}/Ca-Fe oxide	1.034	2.576	+	+	+	-	-
SO_4^{2-}/Mg-Fe oxide	1.293	2.317	+	+	±	-	-

+, acidic color; ±, slightly acidic color; -, basic color

[a.] electronegativity of metal ions

[b.] the difference in electronegativity between oxygen ions and the adjacent metal ions of the support of a sulfated catalyst.

Table 3. Acidic density of the SO_4^{2-}/Sr-Fe oxide samples with various Sr to Fe atomic ratios.

Catalyst	Atomic Ratio[a] Sr : Fe	Surface area (m^2/g)	Total acidity (mmol/g)	D_{BAT}[b] ($\times 10^{-2}$ mmol/m^2)
SO_4^{2-}/Sr-Fe oxide-1	1 : 1.45	9.82±0.10	2.68±0.10	27.29±0.73
SO_4^{2-}/Sr-Fe oxide-2	1 : 2.10	9.58±0.06	2.38±0.11	24.79±0.96
SO_4^{2-}/Sr-Fe oxide-3	1 : 3.33	8.62±0.44	0.91±0.08	10.55±0.45
SO_4^{2-}/Sr-Fe oxide-4	1 : 34.58	7.21±0.33	0.33±0.04	4.50±0.29

[a] the atomic ratio of Sr to Fe was calculated using EDS analysis

[b] acid site density evaluated by using the n-butyl amine titration method

3.2 IR studies of adsorbed oleic acid on catalyst surface

Before sulfate modification, the composite oxides were inactive for the esterification of oleic acid with methanol. The IR spectra of the composite oxides filtrated from the reaction mixture exhibit the characteristic IR bands of physically and chemically adsorbed oleic acid (Figure S3). As directly confirmed by the IR spectra shown in Figure S3, the inactivation of the composite oxides for the esterification of oleic acid can be ascribed to the fact that the catalyst surface was saturated by the chemical and physical adsorbed oleic acids, thereby blocking the active sites present on the catalysts, as the scheme shown in Figure S4.

The IR spectra shown in Figure 5 were taken from the sulfate modified composite oxides filtrated out from the reaction mixture of oleic acid and methanol after 2 hours of the reaction. In the IR spectrum of the used SO_4^{2-}/Mg-Fe oxide, the bands attributed to C-H stretching vibration appear as a weak shoulder of the broad

View Article Online
DOI: 10.1039/C5GC00188A

bands in the region of 3700-2800 cm^{-1}, and the characteristic IR band relating to chemically adsorbed oleic acid at 1743 cm^{-1} is too low to be seen, indicating that grafting sulfate groups efficiently inhibits the bonding of oleic acid on its surface. In contrast to the IR spectrum of the used SO_4^{2-}/Mg-Fe oxide, there is a clear band at 1743 cm^{-1} in the IR spectrum of the used SO_4^{2-}/Sr-Fe oxide and the used SO_4^{2-}/Ca-Fe oxide, indicating that more oleic acid chemically adsorbed on the used SO_4^{2-}/Sr-Fe oxide and used SO_4^{2-}/Ca-Fe oxide rather than on used SO_4^{2-}/Mg-Fe oxide. Moreover, the IR spectrum of the used SO_4^{2-}/Mg-Fe oxide exhibits an intense broad band in the region of 3700-2800 cm^{-1}, and a narrow band at 1636 cm^{-1}, suggesting that its surface is still rich in hydrogen bonded hydroxyl groups (H-OH) and physically adsorbed water. For the IR spectrum of SO_4^{2-}/Sr-Fe oxide, the broad band associated with H-OH observed in the IR spectrum of a fresh SO_4^{2-}/Sr-Fe oxide is displaced by a sharp band at 3465 cm^{-1} in the IR spectrum of a used SO_4^{2-}/Sr-Fe oxide (Figure 5). This could be contributed by the isolated hydroxyl groups (isolated OH)[34]. The transfer in the configuration of surface hydroxyl groups can be interpreted as that the distance of adjacent hydroxyl groups is enlarged after the reaction. When the reaction is conducted over a SO_4^{2-}/Sr-Fe oxide, oleic acids in considerable amount will substitute for a portion of the hydroxyl groups originally bonded to the metal ions without sulfate modification. As the adjacent hydroxyl groups are divided by bonded oleic acids, the hydrogen-bonding interaction is no longer maintained. It can be assumed that oleic acid and the hydroxyl group compete for the binding sites, the Sr ions in particular, on SO_4^{2-}/Sr-Fe oxide during the reaction, resulting in the elimination of hydrogen bonded hydroxyl groups, as seen in Figure S5. Therefore, calcining used SO_4^{2-}/Sr-Fe oxide at 400^{o}C to remove bonded oleic acid and then exposing the treated catalyst to air would thus lead to the recovery of the H-OH on the SO_4^{2-}/Sr-Fe oxide surface (Figure 5). The following conclusion can be proposed with regard to the distribution of adsorbed oleic acid on the SO_4^{2-}/Sr-Fe oxide: incorporating Sr ions would facilitate the adsorption of oleic acid, resulting in the creation of the hydrophobic regions with densely bonded oleic acid.

View Article Online
DOI: 10.1039/C5GC00188A

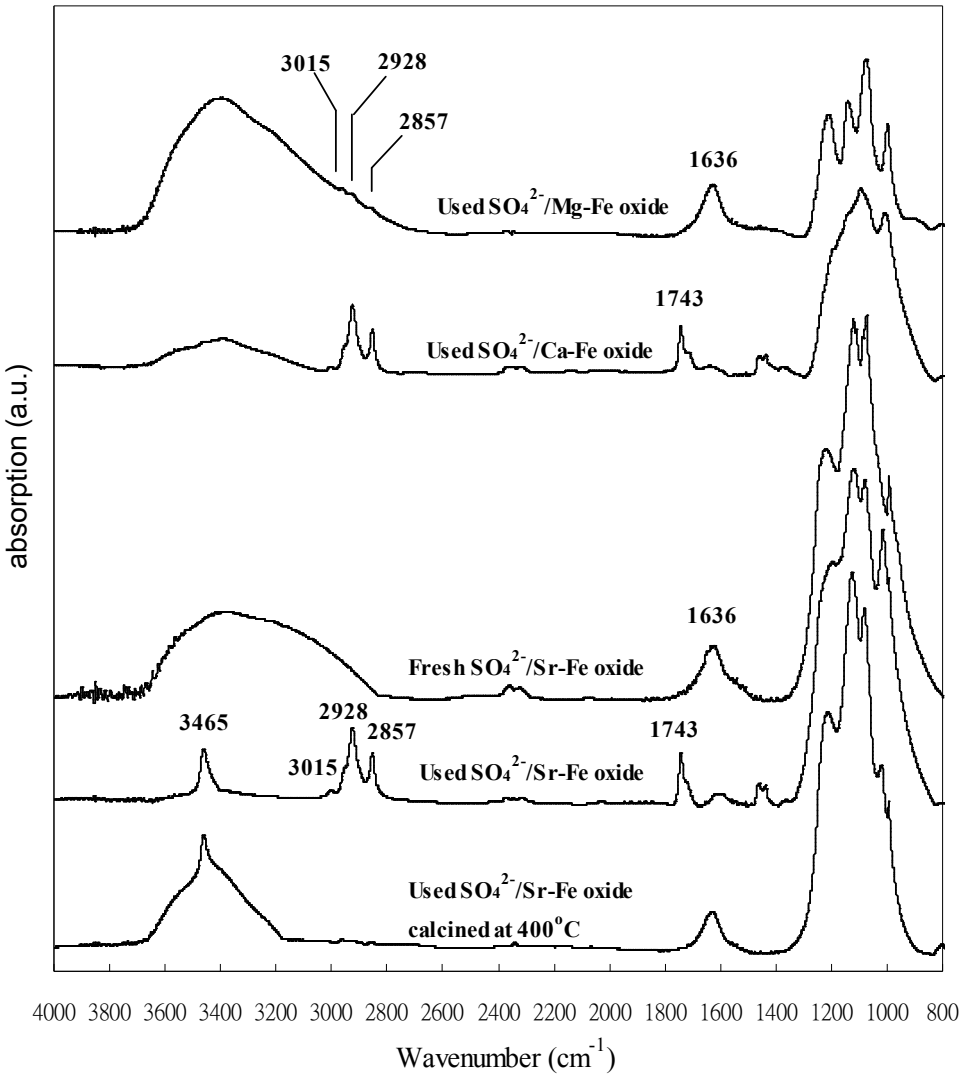

Figure 5. IR spectra of the used sulfated composite oxides, fresh SO_4^{2-}/Sr-Fe oxide and the used SO_4^{2-}/Sr-Fe oxide calcined at 400°C for 2 hours.

3.3 Esterification catalytic reactivity

The catalytic reactivity of the catalysts was evaluated in the esterification of oleic acid with methanol at 100°C. As seen the initial rates (r_0) shown in Table 4, all the sulfated composite oxides exhibit higher reactivity than SO_4^{2-}/Fe_2O_3, indicating that the incorporated alkaline earth metal ions play a key role in the promotion of catalytic reactivity. It was found that both SO_4^{2-}/ZrO_2 and SO_4^{2-}/Sr-Fe oxide exhibited higher catalytic activities for the reaction in comparison with others, and in particular the high catalytic reactivity of SO_4^{2-}/Sr-Fe oxide is comparable with that of SO_4^{2-}/ZrO_2 (Table 4).

Nevertheless, when the reactivity of the active sites was investigated in terms of

View Article Online
DOI: 10.1039/C5GC00188A

turnover frequency (TOF), the results show that the sites present on SO_4^{2-}/Mg-Fe oxide show a similar rate per active site to those on SO_4^{2-}/Sr-Fe oxide (Table 4). These results are obviously contrary to those of the Hammett indicator analysis, in which the acid strength of SO_4^{2-}/Sr-Fe oxide is about two orders of magnitude higher than that of SO_4^{2-}/Mg-Fe oxide (Table 2). To explain these contradictions, it is worth to note again that incorporating Sr cations can facilitate the bonding of oleic acid on the catalyst. Melero *et al.* reported that both Lewis and Brönsted acid sites are able to catalyze the progress of the esterification of fatty acids to produce biodiesel[38]. Brönsted acid sites catalyze the esterification of fatty acids via the protonation of the acid group (-COOH) to give oxonium ions, while the Lewis acid sites catalyze the esterificaiton of fatty acids through the coordination of acid groups on the active sites. The -COOH moiety of an oleic acid is hydrophilic. As a region on the catalyst surface is covered by dense oleic acid, this makes it difficult for the -COOH moiety of an oleic acid to approach the active sites located in this hydrophobic region, further resulting in the deactivation of the active sites. The region with densely bonded oleic acid is denoted as high diffusion barrier zone (Figure 6).

Table 4. Catalytic reactivity of sulfated catalyst samples for the catalysis of the esterification of oleic acid with methanol

Catalyst	Conversion of oleic acid (%)		r_0[a] ($mM \cdot s^{-1} \cdot g^{-1}$ of catalyst)	TOF (min^{-1})[b]
	5 min	120 min		
SO_4^{2-}/Sr-Fe oxide[c]	39.45±1.34	96.97±3.35	3.44±0.12	1.06±0.04
SO_4^{2-}/Ca-Fe oxide	13.09±1.55	77.72±0.87	1.05±0.06	0.44±0.03
SO_4^{2-}/Mg-Fe oxide	8.74±0.37	72.46±1.22	0.76±0.01	1.03±0.02
SO_4^{2-}/ZrO_2	36.50±2.12	98.56±0.34	3.27±0.19	3.11±0.18
SO_4^{2-}/Fe_2O_3	5.77±1.03	63.56±1.35	0.65±0.01	0.62±0.01
SO_4^{2-}/Sr-Fe oxide-1	36.4±0.57	97.86±0.65	3.18±0.05	0.96±0.01
SO_4^{2-}/Sr-Fe oxide-2	33.41±1.41	96.61±1.85	2.92±0.12	1.00±0.04
SO_4^{2-}/Sr-Fe oxide-3	28.50±2.83	87.04±3.06	2.49±0.25	2.22±0.22
SO_4^{2-}/Sr-Fe oxide-4	10.60±0.14	67.88±5.12	0.93±0.01	2.31±0.03

[a] initial rate

[b] initial turnover frequency. TOF is calculated based on the following equation.

$$TOF = \frac{M_{FFA}}{M_{site} \cdot t}$$

Where M_{FFA} and M_{site} are mole of the oleic acid consumed in the reaction per unit time (t) and mole of active sites, respectively. M_{site} is obtained from the result of n-butyl amine titration for each catalyst.

View Article Online
DOI: 10.1039/C5GC00188A

[c] surface Sr:Fe atomic ratio of 1:1.17

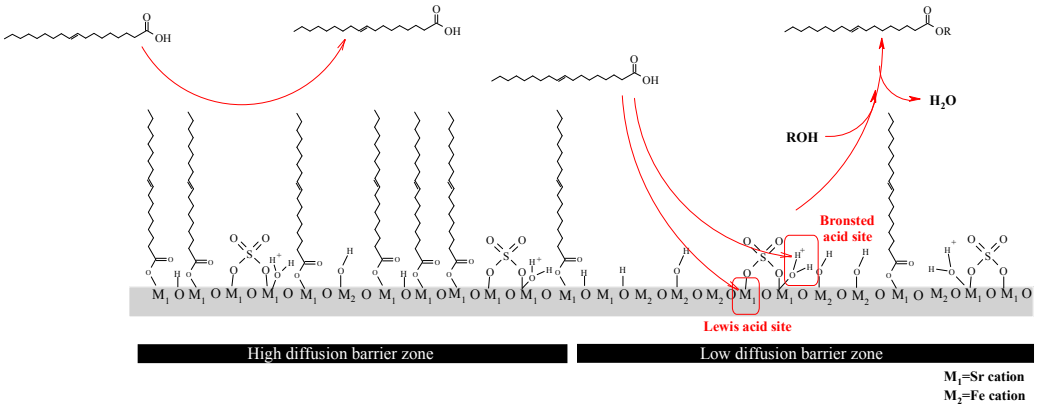

Figure 6. Schematic diagram for explaining the deactivation of the active sites located in the high diffusion barrier zone.

3.4 Effect of the implanted iron cations on the reactivity of SO_4^{2-}/Sr-Fe oxide

In order to study the deactivation mechanism of the active sites present on the sulfated composite oxide surfaces, a series of SO_4^{2-}/Sr-Fe oxides with various Sr to Fe ratio and SO_4^{2-}/SrO were used as the catalysts to individually catalyze the esterification at 100°C. In terms of TOF, the decrease in the surface Sr ion density accompanied an increase in the rate per active site for the catalysts with various Fe/Sr atomic ratio (Table 4). When the atomic ratio of Fe/Sr reaches 34.58 (SO_4^{2-}/Sr-Fe oxide-4), the TOF of SO_4^{2-}/Sr-Fe oxide-4 is comparable to that of SO_4^{2-}/ZrO_2. After the reaction was completed, the density of the oleic acid bonded on the used SO_4^{2-}/Sr-Fe oxide and SO_4^{2-}/SrO samples were measured using TGA, whose profiles are shown in Figure S6 and Figure S7, and TGA results are summarized in Table 5. Obviously, the densities of the bonded oleic acid shown in Table 5 disclose that the content of the bonded oleic acids is proportional to the density of the Sr ions on the catalysts.

The influence of bonded oleic acid on the reactivity of SO_4^{2-}/Sr-Fe oxide was further proved by carrying out the esterification over the SO_4^{2-}/Sr-Fe oxide pre-treated at 700°C (denoted as pre-treated SO_4^{2-}/Sr-Fe oxide) and the used SO_4^{2-}/Sr-Fe oxide recovered at 400°C, respectively. It can be concluded from the IR spectra (Figure 3) and the acidic density data (Table 1) that a portion of bonded sulfate groups remains on pre-treated SO_4^{2-}/Sr-Fe oxide, and the density of the residual sulfate ions is 4.29×10^{-2} mmol/m^2. In comparison to the catalytic reactivity of the catalysts for the esterification, a dramatic decrease in the catalytic reactivity was found on pre-treated SO_4^{2-}/Sr-Fe oxide (Figure 7), while no obvious reactivity loss was observed on the used SO_4^{2-}/Sr-Fe oxide recovered at 400°C (Figure 8). These results suggest that the

View Article Online
DOI: 10.1039/C5GC00188A

deactivation of pre-treated SO_4^{2-}/Sr-Fe oxide is not due to the leaching of the grafted sulfate ions on pre-treated SO_4^{2-}/Sr-Fe oxide. Investigating the reactivity of the active sites in terms of TOF (representing the reactivity per active site of a catalyst) shows that the TOF of SO_4^{2-}/Sr-Fe oxide is about five times higher than that of pre-treated SO_4^{2-}/Sr-Fe oxide (TOF=0.20±0.05 min^{-1}). Considering the nature of the active sites present on SO_4^{2-}/Sr-Fe oxide and pre-treated SO_4^{2-}/Sr-Fe oxide, they should have similar catalytic reactivity for the esterification because these two catalysts have the same crystalline phase and similar surface characteristics (e.g., surface configuration, specific surface area and Fe/Sr ratio), except for the density of the oleic acids bonded on the surfaces during the reaction. It was noted previously that the bonded sulfate groups can prevent the adsorption of oleic acid. In other words, partially removing the covalently bonded sulfate ions at 700°C would create more Sr ions without bonded sulfate ions, and further lead to adsorb more oleic acids during the reaction. These results demonstrate that the decrease in the rate per active site (TOF) for pre-treated SO_4^{2-}/Sr-Fe oxide can be related to the increase in bonded oleic acid density. This finding is in agreement with our previous assumption that the deactivation of the active sites on a SO_4^{2-}/Sr-Fe oxide is due to the creation of the high diffusion barrier zones on the SO_4^{2-}/Sr-Fe oxide with high Sr/Fe ratio (Figure 6). TOF is defined as mol of oleic acid (M_{FFA}) converted in the reaction per mol of active site (M_{site}) per time (t). When the active sites located in high diffusion barrier zone are inactive for the reaction, it leads to the overestimation in the density of the active sites actually catalyzing the reaction, and subsequently causes the underestimation in the TOF of the catalysts. It can be imaged that most active sites on SO_4^{2-}/Sr-Fe oxide-4 surface located in low diffusion barrier zone since SO_4^{2-}/Sr-Fe oxide-4 surface features low Sr/Fe ratio. This explains why the TOF of SO_4^{2-}/Sr-Fe oxide-4 is greater than the TOF of the SO_4^{2-}/Sr-Fe oxides with a low Fe/Sr ratio.

The influence of the implanted Fe ions on the configuration of the covalently bonded sulfate ions as well as on the catalytic reactivity was investigated by carrying out the esterification over SO_4^{2-}/SrO and SO_4^{2-}/Sr-Fe oxide-1. The IR spectra of the catalysts after reaction are shown in Figure S8, showing that a unique IR band at 1455 cm^{-1} only appears in the IR spectrum of used SO_4^{2-}/SrO. This IR band reveals the presence of the polynuclear sulfate ($S_2O_7^{2-}$) produced from the reaction between two adjacent sulfate groups[33]. Since the bonded sulfated groups in large amount still remained on the used SO_4^{2-}/SrO which was recovered at 800°C (Figure S8), the bonded sulfated ion density of $>13.53\times10^{-2}$ $mmol/m^2$ was obtained from the weight loss from 400°C to 800°C in the TGA profile of SO_4^{2-}/SrO (Figure S7). According to the density of the boned sulfate ions, it was found that there are more bonded sulfate ions present on SO_4^{2-}/SrO rather than on SO_4^{2-}/Sr-Fe oxide-1. However, the density of

View Article Online
DOI: 10.1039/C5GC00188A

the acid sites on SO_4^{2-}/SrO ($1.56\pm0.35\times10^{-2}$ mmol/m^2) is about 1/17 of that on SO_4^{2-}/Sr-Fe oxide-1. As seen in Figure S9, SO_4^{2-}/SrO ($r_0=0.55\pm0.14$ mM·s^{-1}·g^{-1} of catalyst) also exhibits much lower reactivity than SO_4^{2-}/Sr-Fe oxide-1 (Figure S9 and Table 4). It can be concluded from these results that the formation of $S_2O_7^{2-}$ will lead to the deactivation of the adjacent active sites, and this conclusion is in agreement with the results reported in previous study[33]. On the SO_4^{2-}/Sr-Fe oxide surface, since sulfate ion tends to bond on Sr cation rather on Fe ion, the formation of polynuclear sulfate species can be efficiently prohibited when the incorporated Sr ions are divided by incorporated Fe ions on the catalyst surface. On the other hand, Sr ion has higher binding ability for oleic acid during the reaction in comparison to Fe ion. Incorporated Fe ions can disperses the distribution of bonded oleic acid on SO_4^{2-}/Sr-Fe oxide, leading to the inhibition of the creation of high diffusion barrier zone.

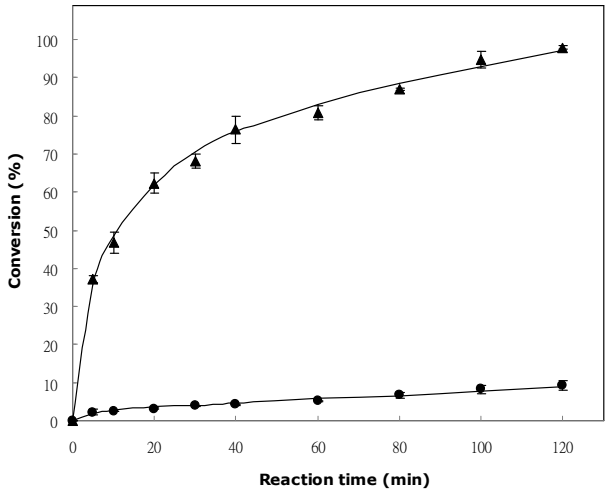

Figure 7. Conversion versus reaction time for oleic acid esterification catalyzed by (▲) SO_4^{2-}/Sr-Fe oxide and by (●) the SO_4^{2-}/Sr-Fe oxide pre-treated at 700°C for 2 hours. The oleic acid esterification was carried out at 100°C.

View Article Online
DOI: 10.1039/C5GC00188A

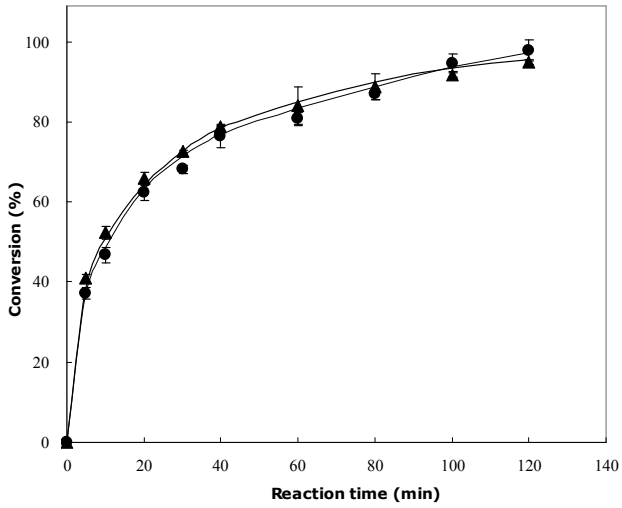

Figure 8. Conversion versus reaction time for oleic acid esterification catalyzed by (●) fresh SO_4^{2-}/Sr-Fe oxide and by (▲) recovered SO_4^{2-}/Sr-Fe oxide obtained by heat-treating the used SO_4^{2-}/Sr-Fe oxide at 400°C. The oleic acid esterification was carried out at 100°C.

Table 5. Density of bonded oleic acid on used SO_4^{2-}/Sr-Fe oxides and used SO_4^{2-}/SrO

Catalyst	Density of bonded oleic acid ($\times 10^{-2}$ mmol/m^2)
Used SO_4^{2-}/Sr-Fe oxide-1	4.30
Used SO_4^{2-}/Sr-Fe oxide-2	1.41
Used SO_4^{2-}/Sr-Fe oxide-3	1.34
Used SO_4^{2-}/Sr-Fe oxide-4	0.12
Used SO_4^{2-}/SrO	7.77

3.5 Reusability study

As noted in the literature, a dramatic loss in catalytic reactivity for a recovered SO_4^{2-}/ZrO_2 is ascribed to the significant leaching of adsorbed sulfate groups in the reaction mixture[2,22,23]. It was found that the conversion of oleic acid decreased from 98.85% to 52.14% after SO_4^{2-}/ZrO_2 was recycled two times (Figure 9). This decline in catalytic reactivity for a sulfated catalyst may be due to sulfate groups leaching in the reaction mixture or the substrate poisoning the active sites. In this case, the decline in activity could be ascribed to the low stability of the surface sulfate groups, because removing the adsorbed species by heat-treating the used SO_4^{2-}/ZrO_2 at 400°C did not recover all catalytic reactivity.

As seen in Figure 9, the catalytic reactivity of SO_4^{2-}/Mg-Fe oxide continuously

View Article Online
DOI: 10.1039/C5GC00188A

declined with an increase in the number of recycles, while the reactivity of SO_4^{2-}/Ca-Fe oxide was almost fully recovered during the first few cycles, and a significant decline in reactivity was found after the 4th cycle. Interestingly, SO_4^{2-}/Sr-Fe oxide can be reused multiple times without an obvious decrease in catalytic reactivity, and 84% catalytic reactivity was recovered after SO_4^{2-}/Sr-Fe oxide was recycled 13 times (Figure 10). It is likely that the stability of a sulfated composite oxide catalyst is related to the alkaline earth metal cations implanted in them. The strength of the covalent bond between metal alkaline earth metal cations and sulfate groups is proportional to the bond polarity, as well as the difference in the electronegativity of metal cations and oxygen anions[39]. As the alkaline earth metal cations have a lower degree of electronegativity, such as Sr, the high bond strength of the covalent bonds between sulfated groups and alkaline earth metal cations may explain why the sulfate groups on SO_4^{2-}/Sr-Fe oxide have more stability in the reaction mixture rather than the sulfate groups on SO_4^{2-}/Ca-Fe oxide and SO_4^{2-}/Mg-Fe oxide. After the 14th cycle, a serious aggregation of the catalysts was observed when the recovered catalyst was re-dispersed in the reaction mixture in the 15th cycle. The serious aggregation of the recovered catalyst is due to that the surface sulfate groups in considerable amount were replaced by covalently bonded oleic acids, leading to a significant change in hydrophilic/hydrophobic property on the catalyst surface.

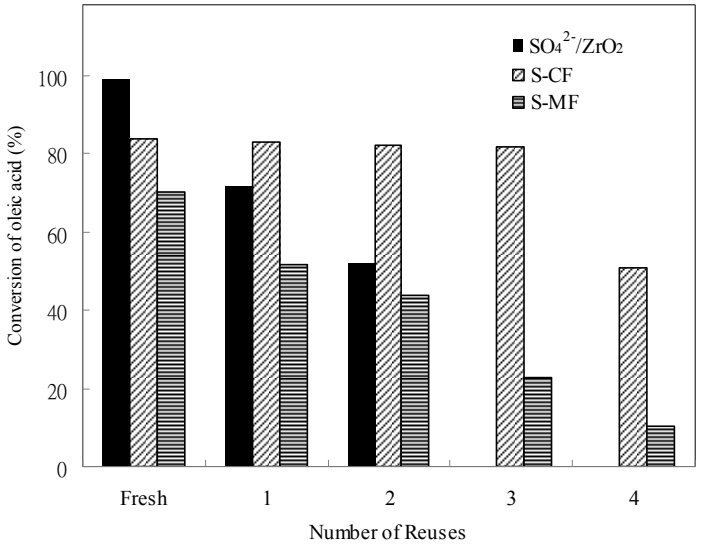

Figure 9. Conversion of oleic acid over recycled catalysts. Reaction conditions: amount of catalyst 0.8g, oleic acid to methanol molar ratio 1:4, reaction temperature 100^{o}C, reaction time 2 hours.

View Article Online
DOI: 10.1039/C5GC00188A

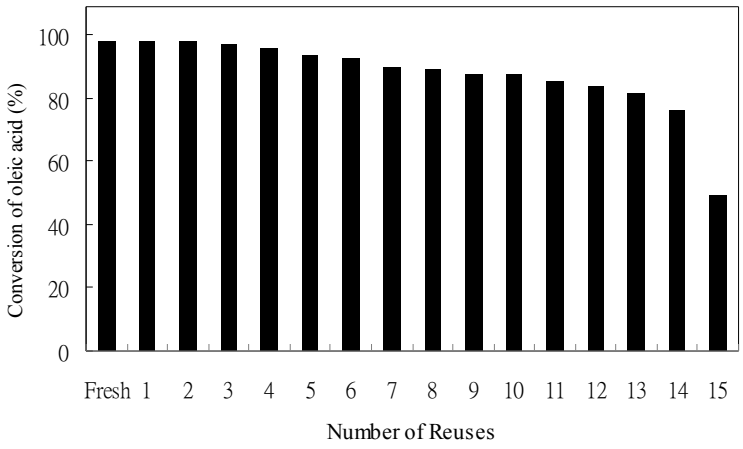

Figure 10. Conversion of oleic acid over recycled SO_4^{2-}/Sr-Fe oxide. Reaction conditions: amount of catalyst 0.8g, oleic acid to methanol molar ratio 1:4, reaction temperature 100^{o}C, reaction time 2 hours.

3.6 Kinetic study

The kinetic parameters of the esterification of oleic acid with methanol over SO_4^{2-}/Sr-Fe oxide were studied using an excess of methanol at different temperatures. The results of Koros-Nowak test indicate that catalytic reactions took place in the kinetic region on the active sites present in the low diffusion barrier zone (Figure S10). The plot of $-\ln(C_a/Ca_0)$ versus reaction time shows a linear relationship, indicating that the reaction is a pseudo first order one with respect to the concentration of oleic acid (C_a), as seen Figure S11. The activation energy (E_a) was determined by fitting the rate constants at 70, 80, 90, 100 and 110^{o}C using Arrhenius plot as given blow:

$$k = A\exp(\frac{-E_a}{RT}) \quad \text{or} \quad \ln k = \ln A - \frac{E_a}{RT}$$

where k is the rate constant, T is the reaction temperature in Kelvin, A is pre-exponential factor, R is the universal gas constant and E_a is the activation energy.

A plot of ln(k) versus 1/T was plotted to determine the E_a based on the slope of the resulting graph shown in Figure S12. The activation energy was found to be 28.53±0.72 kJmol^{-1}. Satyarthi et al.[40] reported that the activation energy of the sulfated zirconia in the esterification of oleic acid with methanol is 24.40 kJmol^{-1}, where is close to the activation energy of SO_4^{2-}/Sr-Fe oxide. The low activation energy can be attributed to the promotion in the acid strength due to the high induction effect of the sulfated ion grafted on Sr cation when the esterification of oleic acid is catalyzed over the active sites located in low diffusion barrier zone on SO_4^{2-}/Sr-Fe oxide. By comparison with the kinetic parameters of the currently used

View Article Online
DOI: 10.1039/C5GC00188A

catalysts in Table S1, SO_4^{2-}/Sr-Fe oxide gives a fairly good performance in catalyzing the esterification of fatty acid with short chain alcohol.

4. Conclusion

This study examined the potential of using alkaline earth metal-ferric composite oxide to enhance the stability of grafted sulfate ions and the catalytic reactivity of the active sites in the esterification of oleic acid with methanol for the production of biodiesel. The results show that acidic strength of the sulfated composite oxides was associated with the electronegativity of the incorporated alkaline earth cation. In particular, SO_4^{2-}/Sr-Fe oxide was classified as a solid superacid, and its acidity function (H_0) determined by Hammett indicators was < -12.70 due to the low electronegativity of Sr cations in comparison with others. It was found that the acid site density and the catalytic reactivity for the esterification are associated with the distribution of the Sr ions incorporated on SO_4^{2-}/Sr-Fe oxide. Examining the catalytic reactivity in term of TOF, the higher TOF value was obtained from the SO_4^{2-}/Sr-Fe oxide with higher surface Fe/Sr atomic ratio. About 85% reactivity could be recovered after SO_4^{2-}/Sr-Fe oxide was recycled 13 times in the esterification of oleic acid with methanol because of the high chemical/thermal stability of the sulfate ions bonded on Sr cations. It can be concluded from these results that implanting Sr ions facilitated the grafting of sulfate ions to create more acid sites, but also facilitated the binding of oleic acid to form high diffusion barrier zones over SO_4^{2-}/Sr-Fe oxide, leading to the deactivation of the active site circulated by densely bounded oleic acid. The catalytic study of SO_4^{2-}/SrO and pre-treated SO_4^{2-}/Sr-Fe at 700^{o}C provides direct evidences to prove that the incorporation of Fe ions on catalyst surface could efficiently suppress the deactivation of the active sites locating in the area with densely bonded oleic acid and the further reaction between adjacently bonded sulfate ions to form polynuclear sulfate.

Acknowledgements

Financial support for this work was provided by Taiwan's National Science Council (Grants No. NSC 103-2221-E-126-017-MY2 and MOST 103-3113-E-006 -006 -).

References

[1] P.D. Patil, V.G. Gude, S. Deng, *Ind. Eng. Chem. Res.*, 2009, **48**, 10850.
[2] E. Lotero, Y. Liu, D.E. Lopez, K. Suwannakarn, D.A. Bruce, J.G. Goodwin, *Ind. Eng. Chem. Res.*, 2005, 44, 5353.
[3] K.-H. Chung, D.-R. Chang, B.-G. Park, *Bioresour. Technol.*, 2008, **99**, 7438.
[4] A.S. Ramadhas, S. Jayraj, C. Muraleedharan, *Fuel*, 2005, **84**, 335.

View Article Online
DOI: 10.1039/C5GC00188A

[5] J. Van Gerpen, M. Canakci, *Am. Soc. Agric. Eng.*, 2001, **44**, 1429.
[6] E. Lotero, Y. Liu, D.E. Lopez, K. Suwannakaran, D.A. Bruce, J.G. Goodwin Jr, *Ind. Eng. Chem. Res.*, 2005, **44**, 5353.
[7] M. Di Serio, M. Cozzolino, M. Giordano, R. Tesser, P. Patrono, E. Santacesaria, *Ind. Eng. Chem. Res.*, 2007, **46**, 6379.
[8] S.A. Ardizzone, P. Beltrame, G. Zuretti, *Appl. Catal. A*, 2006, **314**, 240.
[9] C.M. Garcia, S. Teixeira, L.L. Marciniuk, U. Schuchardt, *Bioresource Technol.*, 2008, **99**, 6608.
[10] J.L. Ropero-Vega, A. Aldana-Pérez, R. Gómez, M.E. Niño-Gómez, *Appl. Catal. A*, 2010, **379**, 24.
[11] L.K. Noda, R.M. de Almeida, L.F.D. Probst, N.S. Gonçalves, *J. Mol. Catal. A*, 2005, **225**, 39.
[12] J.I. Moreno, R. Jaimes, R. Gómez, M.E. Niño-Gómez, *Catal. Today*, 2011, **172**, 34.
[13] Y. Du, S. Liu, Y. Zhang, C. Yin, Y. Di, F.-S. Xiao, *Catal. Letters*, 2006, **108**, 155.
[14] H. Yang, H. Song, H. Zhang, P. Chen, Z. Zhao, *J. Mol. Catal. A*, 2014, **381**, 54.
[15] B. Fu, L. Gao, L. Niu, R. Wei and G. Xiao, *Energ. Fuel.*, 2009, **23**, 569.
[16] L.S. Ling, H. Hamdan, *J. Non-Cryst Solids*, 2008, **354**, 3939.
[17] D. Prasetyoko, Z. Ramli, S. Endud, H. Nur, *J. Mol. Catal. A*, 2005, **241**, 118.
[18] T. Wakayama, H. Matsuhashi, *J. Mol. Catal. A*, 2005, **239**, 32.
[19] B.M. Reddy, M.K. *Chem. Rev.*, 2009, **109**, 2185.
[20] G.D. Yadav, J.J. Nair, *Micropor. Mesopor. Mater.*, 1999, **33**, 1.
[21] K. Arata Solid Superacids. *Adv. Catal.*, 1990, **37**, 165-211.
[22] S. Ardizzone, C.L. Bianchi, V. Ragaini, B. Vercelli, *Catal. Lett.*, 1999, **62**, 59.
[23] A. Corma, H. García, *Catal. Today*, 1997, **38**, 257.
[24] J. Ni, F.C. Meunier, *Appl. Catal. A*, 2007, **333**, 122.
[25] C.-L. Chen, C.-C. Huang, D.-T. Tran, J.-S. Chang, *Bioresour. Technol.*, 2012, **113**, 8.
[26] H.-C. Wang, C.-Y. Wu, C.-C. Chung, M.-H. Lai and T.-W. Chung, *Ind. Eng. Chem. Res.*, 2006, **45**, 8043
[27] H. Ranjan Sahu and G. Ranga Rao, *Bull. Mater. Sci.*, 2000, **23**, 349.
[28] M.L. Guzmán-Castillo, E. López-Salinas, J.J. Fripiat, J. Sánchez-Valente, F. Hernández-Beltrán, A. Rodríguez-Hernández, J. Navarrete-Bolaños, *J. Catal.*, 2003, **220**, 317.
[29] R.M. de Almeida, L.K. Noda, N.S. Gonçalves, S.M.P. Meneghetti, M.R. Meneghetti, *Appl. Catal. A*, 2008, **347**, 100.
[30] A. Mantilla, G. Ferrat, A. López-Ortega, E. Romero, F. Tzompantzi, M. Torres, E. Ortíz-Islas, R. Gómez, *J. Mol. Catal. A*, 2005, **228**, 333.
[31] X. Li, W. Huang, *Energy Source, Part A*, 2009, **31**, 1666.
[32] A.S. Khder, E.A. El-Sharkawy, S.A. El-Hakam, A.I. Ahmed, *Catal. Commun.*, 2008, **9**, 769.
[33] G.D. Yadav, A.D. Murkute, *J. Catal.*, 2004, **224**, 218.
[34] C.-C. Huang, K.L. Hohn, J.R. Schlup, *J. Phys. Chem. C*, 2009, **113**, 11050.
[35] S. Tominaka, T. Momma, B. Scrosati, T. Osaka, *J. Power Sources*, 2010, **195**, 4065.
[36] R.J. Gillespie, T.E. Peel, E.A. Robinson, *J. Am. Chem. Soc.*, 1971, **93**, 5083.
[37] M. Yurdakoç, M. Akçay, Y. Tonbul, K. Yurdakoç, *Turk. J. Chem.*, 1999, **23**, 319.
[38] J.A. Melero, J. Iglesias, G. Morales, *Green Chem.*, 2009, **11**, 1285.
[39] M. S. Chandrasekharaiah, *J. Phys. Chem.*, 1964, **68**, 2020.

View Article Online
DOI: 10.1039/C5GC00188A

[40] J.K. Satyarthi, D. Srinivas, P. Ratnasamy, *Energy Fuels*, 2010, **24**, 2154.

DOI: 10.1039/C5GC00188A

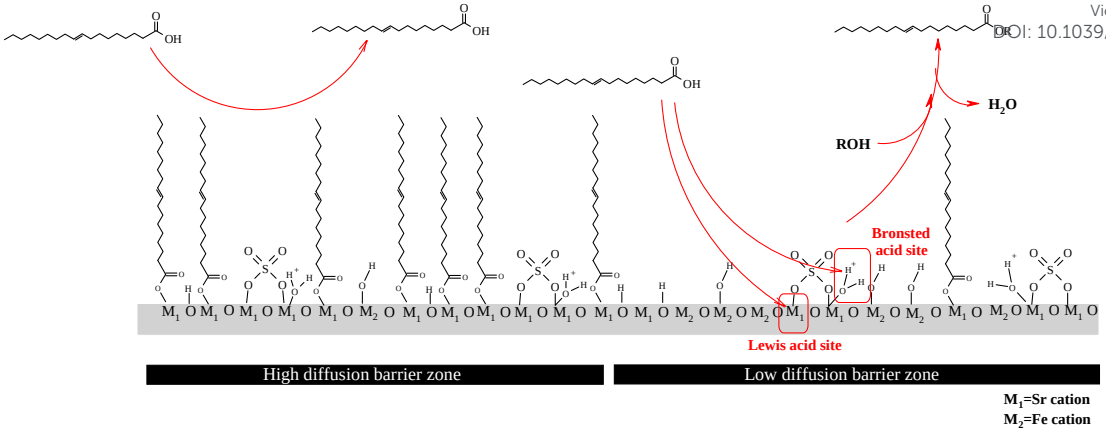

Schematic diagram for explaining the deactivation of the active sites located in the high diffusion barrier zone.